Submilliarcsecond VLBI Using Compact Close Pairs of Radio Sources: Error Analysis

D. D. Morabito
Tracking Systems and Applications Section

The potential accuracy attainable for ΔVLBI positional measurements (submilliarcsecond level) can be reached by simultaneously observing pairs of compact radio sources whose angular separations are smaller than the beamwidth of each antenna. Simultaneous ΔVLBI (SVLBI) enables significant cancellation of measurement errors. Solar plasma is the dominant fluctuating error source in SVLBI positional measurements since there is enhanced cancellation of the troposphere and ionosphere, and complete cancellation of oscillator instabilities. Of the nonfluctuating error sources, errors due to universal time predominate.

By performing SVLBI experiments over several years with many different close pairs of radio sources, limits can be placed on reference-frame stability. Intrinsic properties of the sources, such as source structure and proper motion, will limit measurements. The SVLBI differential phase and corruptive noise sources will be discussed here along with estimated results.

I. Introduction

The advent of phase-stable atomic clocks and digital technology enabled the development of Very Long Baseline Interferometry (VLBI), which offers two orders of magnitude improvement in position determination over what was previously realized by ground-based optical systems. Conventional VLBI is used to measure crustal motion, earth rotation parameters, and relative source positions. The source positions have been measured to milliarcsecond accuracy and rely on the reference frame, defined by the extragalactic radio sources, being stable at the milliarcsecond level.

VLBI is being used by the Deep Space Network for spacecraft navigation (Refs. 1 through 4). By using a technique by which the spacecraft and an angularly nearby quasar are alternately observed, the differential position of the spacecraft can be determined to the milliarcsecond level relative to the quasar reference frame. Quasars from these reference frames have served as reference beacons in ΔVLBI experiments with the Voyager spacecraft (Ref. 2), the Pioneer Venus Orbiter (Ref. 4), and the Viking Orbiter (X X Newhall, private communication). Future applications of this technique will involve performing ΔVLBI between multiple spacecraft associated with a single planet. Such spacecraft include orbiters, landers, flybys, rovers, and balloons.

The potential accuracy attainable for ΔVLBI positional measurements can be reached by simultaneously observing source pairs with small angular separations. The angular sepa-

ration of such a pair must be smaller than the beamwidth of each antenna, so that it can be simultaneously tracked, greatly enhancing cancellation of measurement errors. By using the technique of simultaneous ΔVLBI (denoted SVLBI), there is significant cancellation of errors due to media, baseline, earth rotation parameters, and instrumentation, leaving attributes of the radio sources themselves to dominate (Ref. 5). Such intrinsic source properties include effects due to source structure and perhaps proper motion. By performing SVLBI on selected close pairs of radio sources, limits can be placed on the stability of the celestial reference frame to a precisely determined level. Figure 1 illustrates a comparison of differential position accuracies using conventional VLBI, time-multiplexed ΔVLBI, and SVLBI.

The relative proper motion of close pairs of radio sources can be determined to the several μarcsecond level using SVLBI. Repetitions of such measurements over a period of years will yield values or bounds on proper motions. Estimates of possible proper motion limits run about several μarcseconds/year, which is comparable to the estimated measurement accuracy of SVLBI. The detection of proper motion between two independent quasars would be of great scientific interest to the astronomy community and may have profound implications concerning standard interpretations of cosmological expansion theory. The absence of any detectable proper motion would support the apparent rigidity of the quasar reference frame, and would benefit the spacecraft navigation community.

Previous work using time-multiplexed ΔVLBI and SVLBI on close pairs of radio sources will be addressed here. Shapiro et al. (Ref. 6) estimated the relative position of the radio sources 3C 345 and NRAO 512 with an accuracy of 500 μarcseconds using time-multiplexed ΔVLBI. The relative proper motion of this source pair was bounded to 500 μarcseconds/year. Observations of the close pair 1038+528 have been conducted by Reid et al. (Ref. 7), Marcaide and Shapiro (Ref. 5) and Owen et al. (Ref. 8). Marcaide and Shapiro have measured the angular separation of 1038+528 using SVLBI to accuracies of 3 μarcseconds at X-band and 9 μarcseconds at S-band. The discrepancy found between their S-band and X-band measurements was significant (800 μarcseconds) and was attributed to the wavelength dependent opacity of one component. Gorenstein et al. (Ref. 9) monitored the "double" quasar 0957+56, which is thought to be multiple images caused by an intervening galaxy acting as a gravitational lens. The angular separation between the two components was measured to an accuracy of about 50 μarcseconds. Porcas et al. (Ref. 10) discussed the structure of this double quasar, which was found to be symmetrical and of similar core jet types. Morabito (Ref. 11) demonstrated 30-μarcsecond repeatability in the angular separation of GC 1342+662 and GC 1342+663 in two experiments conducted 4½ months apart using SVLBI with the DSN network.

The differential phase observable in SVLBI measurements will be defined and formulated in Section II. The nonfluctuating error sources will be discussed in Section III, and include errors due to UT1 - UTC, polar motion, baseline, and reference source position. The fluctuating or random noise sources that corrupt the differential phase observable will be discussed in Section IV. These noise sources include solar plasma, the ionosphere, the troposphere, system noise, and the interstellar medium. Source structure will be discussed separately in Section V. The expected accuracy of SVLBI measurements will be discussed in Section VI.

II. Differential Phase Observable

The VLBI instrument is used to simultaneously track two angularly close compact radio sources (see Fig. 2). The observed VLBI phase of source i as a function of time t is expressed by:

$$\phi_i(t) = (2\pi f/c)\,[B_e \cos(H_i(t)) \cos\delta_i + B_z \sin\delta_i] + \psi_i(t) + 2\pi n_i \qquad (1)$$

where

$H_i(t) = \alpha_g(t) + \lambda_b - \alpha_i$ is the hour angle between baseline and source i

f is the observing frequency in Hz

c is the speed of light in m/s

n_i is an integer

B_e is the equatorial component of the baseline in m

B_z is the spin-axis component of the baseline in m

α_i is the right ascension of source i

δ_i is the declination of source i

$\alpha_g(t)$ is the right ascension of Greenwich at time t

λ_b is the baseline longitude

ψ_i represents all dispersive and systematic noise contributions in the phase for source i

The data are recorded on magnetic tapes at each station and brought to a central processing site for cross-correlation. The VLBI software generates a model phase that is differenced from the observed phase (Eq. (1)), yielding a residual phase for source i. The residual phases of the two sources are then differ-

enced. By assuming that source 1 serves as a reference source, the resulting differential VLBI phase between sources 1 and 2 at sample time t_j is expressed by:

$$\Delta\phi(t_j) = (2\pi f/c)\,[B_e \sin H_2(t_j) \cos\delta_2\,\Delta\alpha - B_e \cos H_2(t_j)\,[\Delta\alpha^2/2 \cos\delta_2 + \sin\delta_2\,\Delta\delta] + B_z \cos\delta_2\,\Delta\delta] + F(\Delta\alpha, \Delta\delta) + \Delta\psi(t_j) + 2\pi(n_2 - n_1) \qquad (2)$$

where $H_2(t_j) = a_g(t_j) + \lambda_b - a_2$; a_2 and δ_2 are the right ascension and declination, respectively, of source 2; $\Delta\alpha$ and $\Delta\delta$ are the differential position offsets of right ascension and declination, respectively, for source 2 relative to source 1; $F(\cdot)$ denotes functional dependence on higher order terms of $\Delta\alpha$ and $\Delta\delta$. The differential noise term is expressed as:

$$\Delta\psi(t_j) = \psi_2(t_j) - \psi_1(t_j)$$

The differential phases (Eq. (2)) are input to a weighted-least-squares algorithm where $\Delta\alpha$ and $\Delta\delta$ are determined. The presence of data gaps in the pass may allow integer cycle ambiguities that must be corrected using standard phase connection techniques prior to least-squares fitting. The integer number of cycles, $n_2 - n_1$, can be determined from a preliminary fit and then subtracted from each differential phase measurement. A two-parameter fit can be performed yielding accurate estimates of $\Delta\alpha$ and $\Delta\delta$.

The noise on each measurement of differential phase, $\Delta\psi_j$, is assumed to be uncorrelated with the noise on any other measurement of differential phase $\Delta\psi_k$, $k \neq j$, with each measurement having variance σ_j^2. The noise fluctuates from measurement to measurement because of irregular fluctuations in the noncancelling part of the differential propagation delay and variations in the system noise (thermal conditions). The variance σ_j^2 includes random contributions due to the interstellar medium, solar plasma, the ionosphere, the troposphere, system noise, and perhaps source structure. Because the observations are simultaneous, any oscillator instabilities in the VLBI phase of one source will also manifest itself in the VLBI phase of the other source, and therefore cancel out completely. Most systematic noise sources are expected to significantly cancel, leaving those intrinsic to the radio sources to dominate along with the dispersive noise sources. Nonfluctuating and fluctuating noise sources will be discussed in the following sections.

III. Nonfluctuating Error Sources

This section discusses the propagation of errors in the right ascension and declination components of relative position due to errors in our knowledge of the rotation of the earth (UT1 - UTC), the position of the pole, the baseline, and the coordinates of the reference source. These error sources are considered nonfluctuating in that they do not contribute stochastically within an experiment but do contribute systematically. For this analysis, it is assumed that the observations are performed on the Goldstone-to-Madrid baseline and that the measurements are equally spaced over a diurnal period. The estimated errors presented may vary depending upon the hour angle range covered by the pass. However, they should be representative of errors incurred during actual experiments. A similar analysis is presented by Shapiro et al. (Ref. 6).

A. UT1-UTC and Polar Motion Errors

Using equation (2) and the above assumptions, errors in universal time, dt_u, and errors in polar motion parallel to the equatorial baseline component, dP_q, and perpendicular to the equatorial baseline component, dP_t, map into errors of estimated differential right ascension and differential declination as follows:

$$d\Delta\alpha \approx \Delta\alpha\, B_z/B_e\, dP_q - (\Delta\delta \tan\delta_2 + \Delta\alpha^2/2)\,(\omega_e\, dt_u - B_z/B_e\, dP_t)$$

$$d\Delta\delta \approx \Delta\delta\, B_z/B_e\, dP_q + \Delta\alpha \cot\delta_2\,(\omega_e\, dt_u - B_z/B_e\, dP_t)$$

For sources near the celestial equator, $d\Delta\alpha$ becomes negligible while $d\Delta\delta$ becomes significant. For sources near the pole, $d\Delta\alpha$ becomes significant while $d\Delta\delta$ becomes negligible. One millisecond is the typical BIH uncertainty of dt_u, but excursions of 4 milliseconds from quoted BIH values occasionally occur (Ref. 12). For BIH uncertainties of UT1 - UTC, positional errors can run up to 200 μarcseconds in right ascension at 80 degrees declination. Errors in positional measurements due to errors in UT1 - UTC can be reduced by solving for UT1 - UTC using VLBI. VLBI determined values of UT1 - UTC are accurate to 0.2 milliseconds.

The error in differential right ascension or declination due to BIH polar motion uncertainties of 0.015 arcseconds in each component is very small ($\approx$2 μarcseconds). For the Goldstone-to-Madrid baseline, error contributions due to UT1 - UTC clearly dominate over those of polar motion and, (as shown

below), the other nonfluctuating error sources. Baselines with larger ratios of north-south to equatorial components will have larger relative source position errors due to errors in polar motion.

B. Baseline Errors

The errors in right ascension and declination due to the errors in the baseline are given by:

$$d\Delta\alpha = -\Delta\alpha\, dB_e/B_e$$

$$d\Delta\delta = -(\Delta\delta + \Delta\alpha^2/2 \cot\delta_2)\, dB_e/B_e$$

Typical DSN baseline errors of 0.1 to 1.0 m will limit errors in angular separation to <10 μarcseconds for passes involving intercontinental baselines.

C. Reference Source Position Errors

The errors in relative right ascension and declination due to errors in the reference source position ($d\alpha_2$, $d\delta_2$) can be expressed by:

$$d\Delta\alpha = \Delta\alpha \tan\delta_2\, d\delta_2 + (\Delta\delta \tan\delta_2 + \Delta\alpha^2/2)\, d\alpha_2$$

$$d\Delta\delta = (-\Delta\delta \cot\delta_2 + \Delta\alpha^2/2)\, d\delta_2 + (\Delta\alpha \cot\delta_2)\, d\alpha_2$$

For sources near the pole, $d\Delta\alpha$ becomes significant and $d\Delta\delta$ insignificant, while for sources near the celestial equator, $d\Delta\alpha$ becomes insignificant with $d\Delta\delta$ becoming significant. Errors in angular separation due to errors in reference source position (1 milliarcsecond) are limited to <10 μarcseconds for reasonable source declinations.

IV. Fluctuating Error Sources

A. Solar Plasma

The scatter in the differential phase (Eq. (2)) due to solar plasma (in radians) is shown by Callahan (Ref. 13) to be:

$$\sigma_{\Delta\psi} = 1.1\,(1/f)\,(L/v)^{0.75}\,F(\varepsilon) \qquad (3)$$

where f is the observing frequency in GHz, v is the propagation velocity of the solar plasma (400 km/s), L is the plasma scale size in km and $F(\varepsilon)$ is given by:

$$F(\varepsilon) = \begin{cases} [10 \sin\varepsilon]^{-1.3} & 0 < \varepsilon \leqslant 90^\circ \\ 10^{-1.3} & \varepsilon > 90^\circ \end{cases}$$

where ε is the elongation angle between sun and source pair.

Figure 3 illustrates the ray-path geometry between stations and sources at the solar plasma scale height. The separation of ray paths at the 1 AU (1.5×10^8 km) scale height between the two sources as seen from one station is $S = (1.5 \times 10^8)\,\Delta\theta$ km where $\Delta\theta$ is the angular separation in radians between the two sources. If B, the projected baseline length perpendicular to the source direction, is greater than S, then cancellation is between ray paths of the sources as seen from one station; hence, $L = S$ in Eq. (3). When $B < S$, then cancellation is across ray paths between stations as seen from each source; hence, $L = B$ in Eq. (3).

The effects of the solar plasma on the SVLBI phase for $B < S$ are the same as for time-multiplexed ΔVLBI or conventional VLBI. The solar plasma becomes a dominant error source for SVLBI because of the enhanced cancellation of other error sources that dominate in the other VLBI systems. The contribution of the solar plasma to the differential phase error is about 0.23 radians at S-band for the Goldstone-to-Madrid baseline under nighttime conditions with source pairs having $\Delta\theta \gtrsim 0.2$ arcminutes. For source pairs with $\Delta\theta \lesssim 0.2$ arcminutes, the solar plasma contribution to the phase error decreases as $\Delta\theta$ decreases. Solar plasma effects take place over time scales of 0.1 to 100 seconds depending upon solar elongation angle.

B. Ionosphere

For two sources separated by $\Delta\theta$ radians in the sky, we estimate the ionospheric effect on the differential phase. At the ionospheric scale height of 350 km, the separation between ray paths is 350 $\Delta\theta$ km. From Ref. 14, the relative fluctuations in electron density are given by:

$$\delta n/n = 5.9 \times 10^{-4}\,(350\Delta\theta)^{0.83} \qquad (4)$$

The ionosphere path delay I, in meters, is related to the observing frequency f in GHz, and the total electron content TEC, in 10^{17} electrons/m^2, by:

$$I = (4.03/f^2)\,TEC \qquad (5)$$

TEC is typically between 1 and 2 at night and as high as 10 during the day.

The fractional fluctuation in plasma density is assumed to be approximately equal to the fractional fluctuation in path delay:

$$\delta I/I \approx \delta n/n \qquad (6)$$

where δI is the delay fluctuation corresponding to the ray-path separation between the two sources at the ionospheric scale

height as seen by one station. By substituting Eqs. (4) and (5) into Eq. (6), we get:

$$\delta I = (0.307/f^2)\, TEC\, (\Delta\theta)^{0.83}$$

The differential phase scatter in radians due to ionosphere is expressed by:

$$\sigma_{\Delta\psi} = 6.4/f \sqrt{(TEC_1)^2 + (TEC_2)^2}\ \Delta\theta^{0.83}$$

where TEC_i is the total electron content present at station i.

The ray-path separations between sources are much smaller for SVLBI than the effective scale sizes present for time-multiplexed ΔVLBI or conventional VLBI. For these conventional VLBI systems, cancellation is over scale sizes on the order of 100 km. Typical ionospheric phase fluctuations can run about four radians over 600 s of observation time at S-band. Conventional VLBI is usually limited by the ionosphere at S-band. For SVLBI, the ionospheric contribution to the differential phase error is about 0.04 radians at S-band for a source separation of 7 arcminutes assuming nighttime conditions. Ionospheric effects are expected to take place over time scales of 1 second and above.

C. Troposphere

From power-law fits to the phase structure function at 5 GHz (Ref. 15), the tropospheric contribution to the phase uncertainty, in radians, can be approximated by:

$$\sigma_{\Delta\psi} \approx 0.44\, \Delta\theta^{0.7}$$

where $\Delta\theta$ is the source separation in radians. All parameter dependence is neglected except for source separation. The ray-path separation at the 6000-m scale height defines the appropriate scale sizes for the troposphere.

The troposphere contributes about ≈ 0.4 radians of phase noise in conventional VLBI systems. Because of the very small separation of the ray paths between the two sources, the troposphere effectively cancels out along with the ionosphere, leaving other noise sources to dominate in SVLBI experiments. The ray-path separation is ≈ 14 m for source pairs separated by 8 arcminutes using SVLBI, corresponding to a phase uncertainty of about 0.006 radians.

D. System Noise

The error on differential phase due to system noise is now discussed. Let $\Delta\tau$ be the differential delay between the correlator outputs of the two sources and W be the recording bandwidth. The signal of one component is uncorrelated with the signal of the other component when the source separation is sufficient such that $\Delta\tau > 1/W$. The signals are therefore separable in delay and reside on different bits. The differential phase uncertainty is the RSS of the individual source VLBI phase uncertainties and is given by (in radians):

$$\sigma_{\Delta\psi} = \sqrt{(SNR_1)^{-2} + (SNR_2)^{-2}}$$

where the signal-to-noise ratio for source j is estimated as follows:

$$SNR_j = 0.2\, S_j\, D_1\, D_2 \sqrt{(\varepsilon_1\, \varepsilon_2/T_1\, T_2)\, WT} \cdot \sqrt{\exp\left(-0.69\, [\Delta_{j1}^2/\theta_1^2 + \Delta_{j2}^2/\theta_2^2]\right)}$$

where S_j is the correlated flux density in Janskys of source j; D_i, ε_i, T_i, and θ_i are the diameter (m), efficiency, system noise temperature (K), and half-power beamwidth, respectively, of antenna i; W is the system bandwidth (MHz); T is the total observation time (sec); and Δ_{ji} is the angular separation between source j and the pointing center for antenna i. It is usually appropriate to use the centroid of the two sources to point each antenna in order to minimize complications ($\Delta_{1i} = \Delta_{2i}$).

The contribution to the differential phase noise due to the system noise ranges from negligible to significant depending on source strengths, system parameters, and observation time. System noise effects are characterized by rapid fluctuations as opposed to media-induced noise effects, which fluctuate more slowly. The system noise effects for reasonably small pointing offsets are the same for both conventional VLBI and SVLBI.

E. Interstellar Medium

The effects of the interstellar medium (ISM) are the least understood of all medium-related error sources affecting the differential phase observable. Scale sizes on the order of the baseline length are assumed. θ is assumed to be the scattered angular size of a source caused by diffractive interference of the ISM. A circular Gaussian source of half-power width θ in radians yields the fringe visibility given by:

$$\gamma(B, \theta, f) = \exp\left(-0.5\, (4.45\, f\, \theta\, B)^2\right) \qquad (7)$$

where B is the baseline projected against the source in meters, and f is the observing frequency in GHz. The structure function, D_ψ, of the fringe phase, ψ, can be determined from Eq. (7) using the relation:

$$\gamma(B, \theta, f) = \exp\left(-0.5\, D_\psi(B, \theta, f)\right) \qquad (8)$$

For galactic latitudes b greater than 5 degrees away from the galactic plane, the angle θ in radians has been estimated by Cordes (private communication) to be:

$$\theta \approx 0.41 \times 10^{-8} f^{-2.2} |\sin b|^{-0.6} \quad (9)$$

Assuming similar effects in the VLBI phase for both sources, the differential VLBI phase uncertainty due to the ISM is approximated using Eqs. (7) through (9) by:

$$\sigma_{\Delta\psi} \approx 1.90 \times 10^{-8} B f^{-1.2} |\sin b|^{-0.6} \qquad (b > 5 \text{ deg}) \quad (10)$$

For galactic latitudes below 5 degrees, the scatter size θ becomes more complicated and more strongly a function of galactic longitude.

Equation (10) with the Goldstone-Madrid baseline (B = 8.4×10^3 km) and b = 90 deg yields 0.058 radians of phase noise at S-band, and 0.012 radians of phase noise at X-band. ISM effects relate to fluctuation times of 100 to 1000 s and above, which are higher than those of the other error sources discussed. For low galactic latitudes, the ISM may dominate the differential phase noise. At higher galactic latitudes, the ISM is dominated by the solar plasma. Because the baseline defines the scale size, the effects of the ISM are the same for both conventional VLBI and SVLBI.

V. Structure Effects

Complex structure in one or both components of a close pair can contribute to erroneous angular separation measurements. Structure effects typically manifest themselves as position offsets due to the apparent motion of the brightness center of a source. Brightness distributions could change detectably at different epochs and lead to different relative position measurements resulting in the erroneous detection of proper motion. Marcaide and Shapiro (Ref. 5) have demonstrated that astrometry can be perfected down to the limits placed only by the brightness distribution of the sources. The milliarcsecond dimensions of the sources to which the VLBI observations are sensitive can be contrasted to the submilliarcsecond precision of SVLBI.

The magnitude of source structure effects on SVLBI measurements are expected to: (1) be zero for two perfect point sources, (2) be bounded by the fringe spacing of the interferometer for unresolved sources, and (3) possibly exceed the fringe spacing for resolved sources.

Prospective source pairs to be used for testing reference – frame stability should be known unresolved sources. SVLBI estimates of the differential source position over a many year period using several such source pairs will yield statistical bounds on reference-frame stability. Significant movement of the differential position measurements outside of the statistical uncertainties could be interpreted as detectable proper motion over that time period. Present estimates on the bounds of proper motion assuming current cosmological theories range upwards to several μarcseconds per year.

Time scales of structure effects can be estimated by comparing measurements between segments of an experiment and between different experiments over different time epochs. By performing several experiments over many years, these time scales can be statistically determined and cross-compared for different source pairs. Structure effects and proper motion can be sorted out more accurately using this data.

VI. Expected SVLBI Accuracy

To study limits of positional measurement accuracy, a given close pair should be monitored over a continuous several-hour pass and at regular intervals. A several-hour pass will insure high accuracy measurements while continuity will provide less difficulty in solving for cycle ambiguities. By repeating measurements over time, reference-frame stability can be tested and limits inferred. Cancellation of systematic error sources is expected to be sufficiently complete, so that any mismodeling may not perceptably bias the results. Structure effects can be minimized by producing radio brightness maps of both sources using a network of several antennas.

Six known angularly close pairs of radio sources appear in Table 1 along with the 1950.0 source positions, correlated flux densities, angular separations, and galactic latitudes. In all six cases, the angular separation between components is less than 7 arcminutes. These source pairs can be simultaneously observed at S-band using DSN baselines. The VLBI sensitivity of a pair of 64-m antennas using the MARK II recording system (4 Mb/s) is ~20 mJy for integration times of 100 s. Therefore, all source pairs listed in Table 1, except 0532-05, can be observed using S-band with this configuration.

Table 2 displays estimated S-band (2.29 GHz) fluctuating phase noise contributions for the source pairs listed in Table 1. 0532-05 is not included here since it is probably self-absorbed at S-band. The Goldstone-to-Madrid baseline is assumed using a 6-hour pass at nighttime. The flux densities used to estimate the system noise effects at S-band are assumed to be those given in Table 1. The sensitivity of an interferometer consisting of two 64-m antennas is sufficient to detect both components of the source pairs listed. By performing SVLBI, the ionosphere and troposphere significantly cancel leaving the solar plasma to dominate. Note that the other noise contributions listed in the table are smaller by comparison, except

those for 2016+112, which are dominated by the ISM. The ISM is expected to dominate for source pairs with smaller galactic latitudes. Figure 4 displays estimated differential phase and source separation errors versus angular source separation for S-band using the above configuration.

Table 3 displays the corresponding estimates of fluctuating phase noise for X-band observations (8.42 GHz). 3C 66 is not included here since the source separation is larger than the X-band beamwidths of the available DSN antennas. Since GC 1342+66 has an angular separation greater than a 64-m antenna beamwidth, a pair of 34-m antennas has been assumed in order to accommodate simultaneous observations. The flux densities used to estimate the system noise effects at X-band are assumed to be those given in Table 1. From Table 3, the solar plasma is shown to be the dominating error source at X band ($\approx$ 0.064 radians), except for the cases of 0532-05, where the system noise (0.082 radians) dominates, and 2016+112, where the ISM dominates. The system noise contribution for 0532-05 can be reduced to 0.022 radians using Mark III recording. Figure 5 displays estimated differential phase and source separation errors versus angular source separations for X-band using the above configuration.

An advantage of using X-band is that the plasma media contributions are significantly reduced compared to the S-band case. It is obviously more advantageous to observe at X-band if antenna beamwidths and source strengths permit. A disadvantage of using X-band is that the antenna beamwidth may be smaller than the angular separations of some source pairs. Thus simultaneous observations are not possible without resorting to smaller antennas (larger beamwidths) at the cost of lower sensitivity.

Estimated uncertainties for observing the source pair GC 1342+66 under the conditions of Tables 2 and 3, are 0.24 radians ($\approx$22 μarcseconds) at S-band, and 0.066 radians ($\approx$5 μarcseconds) at X-band. The estimated S-band values of random phase uncertainty (0.24 radians) are in agreement with measured values (0.17 radians) (Ref. 11). Figure 6 displays the S-band error budget for observing GC 1342+66. The random errors (ie., solar plasma) clearly dominate over the systematic errors. Figure 7 is the corresponding X-band error budget for observing GC 1342+66. Here the random errors are dominated by those due to UT1 - UTC. It is therefore advisable to solve for UT1 - UTC using VLBI so that angular separation errors can be further reduced.

VII. Conclusion

By performing SVLBI on an angularly close source pair, the source separation can be estimated to the submilliarsecond level (and approach the μarcsecond level) because of the enhanced cancellation of error sources. This is a great improvement over conventional VLBI methods. The differential phase observable and the error sources affecting angular separation measurements have been discussed. The nonfluctuating error sources include errors due UT1 - UTC, polar motion, baseline, and reference source position. The fluctuating error sources include the interstellar media, solar plasma, ionosphere, troposphere, and system noise. Source structure effects have been discussed along with the expected accuracies using this technique.

Solar plasma is the dominant error source for SVLBI measurements because of the enhanced cancellation of the troposphere and ionosphere. For weaker source pairs, the system noise may start to dominate. For sources with low galactic latitudes, the ISM may start to dominate.

By performing SVLBI experiments over several years with many different close pairs of radio sources, limits can be placed on reference-frame stability. Intrinsic properties of the sources, such as source structure and proper motion which limit measurements, can then be more fully understood. SVLBI will therefore provide a useful tool for testing long-term reference-frame stability.

Acknowledgements

I would like to thank D. Trask, K. M. Liewer, G. H. Purcell, A. E. Niell, J. W. Armstrong, R. A. Preston, S. C. Wu, D. L. Jauncey, P. S. Callahan, and T. P. Yunck for many interesting discussions.

References

1. Melbourne, W. G., Curkendall, D. W., "Radio Metric Direction Finding: A New Approach to Deep Space Navigation," AAS/AIAA Astrodynamics Specialist Conference Paper, presented at Jackson Hole, Wyoming, Sept. 7-9, 1977.

2. Border, J. S., Donivan, F. F., Finley, S. G., Hildebrand, C. E., Moultrie, B., and Skjerve, L. J., "Determining Spacecraft Angular Position with ΔVLBI: The Voyager Demonstration," paper 82-1471 presented at AIAA/AAS Astrodynamics Conference, San Diego, California, August 1982.

3. Brunn, D. L., Preston, R. A., Wu, S. C., Siegel, H. L., Brown, D. S., "ΔVLBI Spacecraft Tracking System Demonstration: Part I. Design and Planning," *DSN Progress Report 42-45*, p. 111. Jet Propulsion Laboratory, Pasadena, Calif., 1978, p. 111.

4. Esposito, P. B., Donivan, F. F., Finley, S. G., Newhall, X X, Smith, C. B., Wu, S. C., "Narrowband Differential Interferometry Applied to Pioneer Venus Orbiter," paper presented at AAS/AIAA Astrodynamics Specialist Conference held at Lake Placid, New York, Aug. 22-25, 1983.

5. Marcaide, J. M., and Shapiro, I. I. "High Precision Astrometry Via Very-Long Baseline Radio Interferometry: Estimate of the Angular Separation Between the Quasars 1038+528A and B," *Astronomical Journal*, Vol. 88, 1983, p. 1133.

6. Shapiro, I. I., Wittels, J. J., Counselman, C. C. III, Robertson, D. S., Whitney, A. R., Hinteregger, H. F., Knight, C. A., Rogers, A. E. E., Clark, T. A., Hutton, L. K., Niell, A. E., "Submilliarcsecond Astrometry Via VLBI. I. Relative Position of the Radio Sources 3C 345 and NRAO 512," *Astronomical Journal*, Vol. 84, 1979, p. 1459.

7. Reid, M. J., Owen, F. N., Shaffer, D. B., Kellermann, K. I., Witzel, A., "Quasar Proper Motion Study of 1038+528," *B.A.A.S.*, Vol. 12, 1980, p. 497.

8. Owen, F. N., Wills, B. J., Wills, D., "A Close Pair of Radio-emitting Objects," *Ap. J.*, Vol. 235, No. L59, 1980.

9. Gorenstein, M. V., Shapiro, I. I., Cohen, N. L., Falco, E., Kassim, N., Rogers, A. E. E., Whitney, A. R., Preston, R. A., Rius, A., "VLBI Observations of the "Twin Quasar" 0957+56A, B," *B.A.A.S.*, Vol. 12, 1980, p. 498.

10. Porcas, R. W., Booth, R. S., Browne, I. W. A., Walsh, D., Wilkinson, P. N., "VLBI Structures of the Images of the Double QSO 0957+561," *Nature*, Vol. 289, 1981 p. 758.

11. Morabito, D. D., "Submilliarcsecond VLBI Observations of the Close Pair GC 1342+662 and GC 1342+663", TDA Progress Report 42-77, January-March, 1984.

12. Eubanks, T. M., Steppe, J. A., Spieth, M. A., "The Accuracy of Radio Interferometric Measurements of the Earth Rotation," *Nature*, (Submitted).

13. Callahan, P. S., "An Analysis of Viking S-X Doppler Measurements of Solar Wind Columnar Content Fluctuations," *The DSN Progress Report 42-44*. Jet Propulsion Laboratory, Pasadena, Calif., April 1977.

14. Phelps, A. D. R., Sagalyn, R. C., "Plasma Density Irregularities in the High-Latitude Top-Side Ionosphere," *J.G.R.*, Vol. 81, No. 515, 1976.

15. Armstrong, J. W., Sramek, R. A., "Observations of Tropospheric Phase Scintillations at 5 GHz on Vertical Paths," *Radio Science*, Vol. 17, 1982, p. 1579.

16. Morabito, D. D., Preston, R. A., Williams, J. G., Faulkner, J., Jauncey, D. L., and Nicolson, G. D., "A Full-Sky VLBI Survey at 2.29 GHz," to be published in the *TDA Progress Report.*

17. Moran, J. M., Garay, G., Reid, M. J., Genzal, R., "A Compact Radio Source Associated with the Becklin-Neugebauer Object," *B.A.A.S.* Vol. 13, 1981, p. 852.

18. Lawrence, C. R., Schneider, D. P., Schmidt, M., Bennett, C. L., Hewitt, J. N., Burke, B. F., Turner, E. L., Gunn, J. E., "Discovery of a New Gravitional Lens System," *Science*, Vol. 223, No. 4631, 1984, p. 46-49.

Table 1. Six known angularly close source pairs

Source	Right ascension, h m s	Declination, deg m s	Correlated flux density,[a] Jy	Angular separation, arcmin	Galactic latitude, deg
3C 66A	02 19 29.99	42 48 29.6	0.27 +/-0.05	6.4	-17
3C 66B	02 20 01.73	42 45 54.6	0.09 0.01		
0532-05A	05 32 46.65	-05 24 16.5	0.008[b] 0.0007	0.2	-19
0532-05B	05 32 47.43	-05 24 18.9	0.004[b] 0.0007		
0957+561A	09 57 57.3	56 08 22.9	0.026[c] 0.005	0.1	48
0957+561B	09 57 57.4	56 08 16.9	0.020[c] 0.005		
1038+528A	10 38 43.16	52 49 09.64	0.26 0.03	0.6	55
1038+528B	10 38 45.27	52 49 37.6	0.15[d] 0.01		
GC 1342+662	13 42 17.90	66 17 27.8	0.34 0.04	4.4	50
GC 1342+663	13 42 41.03	66 21 12.9	0.65 0.07		
2016+112A	20 16 55.47	11 17 46.56	0.056[e] 0.003	0.057	-14
2016+112B	20 16 55.27	11 17 45.07	0.062[e] 0.003		

[a]All measurements are at 13-cm wavelengths from Ref. 16, except where otherwise noted.
[b]Reference 17, at 2 cm.
[c]Reference 10, at 18 cm.
[d]Reference 8, at 13 cm.
[e]Reference 18, at 20 cm.

Table 2. S-band estimated phase uncertainties (radians)[a]

Source pair	Solar plasma	Ionosphere	Troposphere	System noise	ISM	RSS
3C 66	0.23	0.04	0.005	0.003	0.12	0.26
0957+561	0.14	0.0014	0.0003	0.018	0.069	0.16
1038+528	0.23	0.006	0.001	0.002	0.065	0.24
GC 1342+66	0.23	0.032	0.004	0.001	0.068	0.24
2016+112	0.094	0.00085	0.0002	0.007	0.14	0.17

[a]These estimates assume the Goldstone-to-Madrid baseline, an observing time of 6 hours, and nighttime conditions. The system noise contribution assumes two 64-m antennas with 0.5 efficiencies, 25-K system temperatures, and Mark II recording. All estimates are based on the data found in Table 1; source structure effects neglected.

Table 3. X-band estimated phase uncertainties (radians)[a]

Source pair	Solar plasma	Ionosphere	Troposphere	System noise	ISM	RSS
0532-05	0.064	0.001	0.0005	0.082	0.024	0.11
0957+561	0.039	0.0004	0.0003	0.018	0.014	0.045
1038+528	0.064	0.002	0.001	0.002	0.014	0.066
GC 1342+66	0.064	0.008	0.004	0.0035	0.014	0.066
2016+112	0.026	0.00023	0.0002	0.007	0.029	0.040

[a]These estimates assume the Goldstone-to-Madrid baseline, an observing time of 6 hours, and nighttime conditions. The system noise contribution assumes two 64-m antennas with 0.5 efficiencies, 25-K system temperatures, and Mark II recording, except for GC 1342+66 where we assume two 34-m antennas in order to accommodate simultaneous observations. All estimates are based on the data found in Table 1; source structure effects neglected.

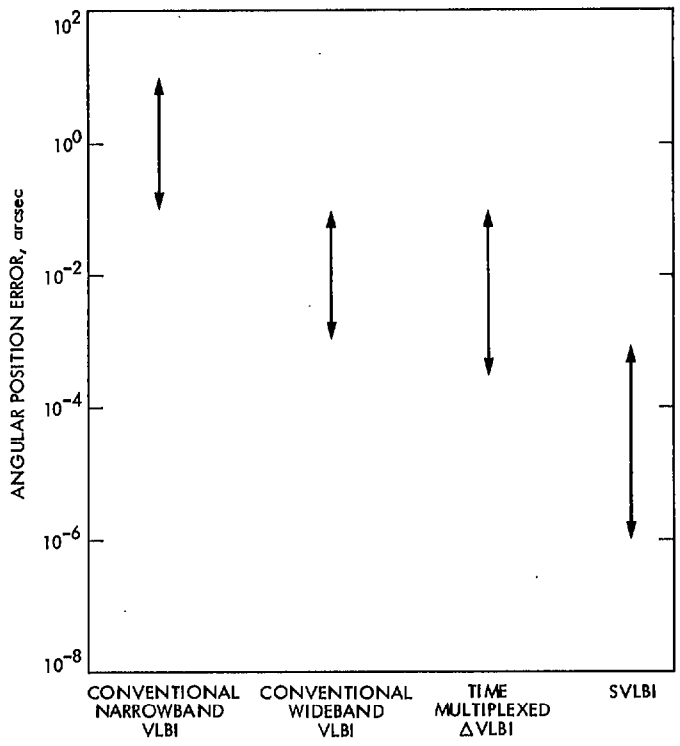

Fig. 1. VLBI system comparison

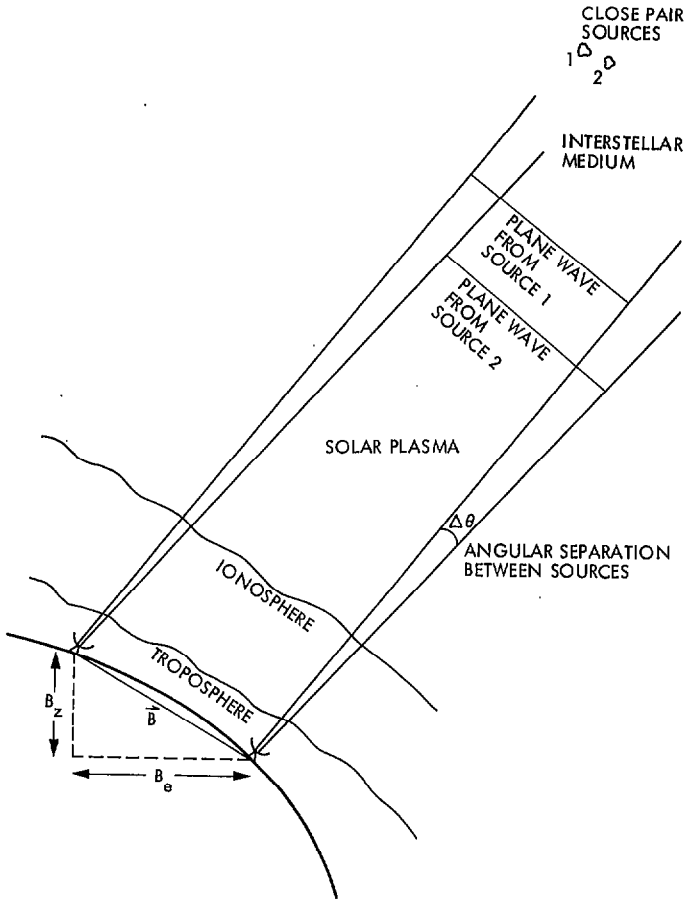

Fig. 2. Basic SVLBI geometry

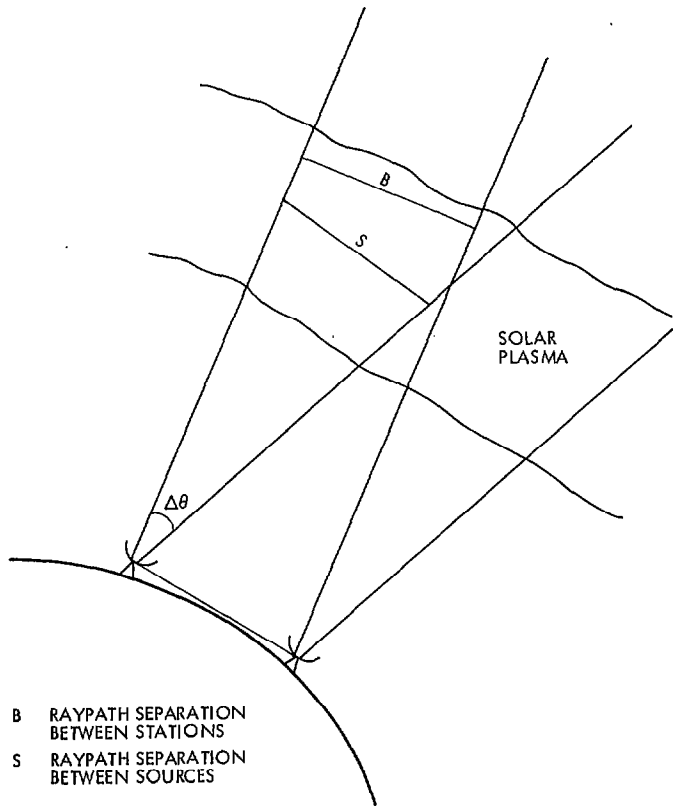

Fig. 3. Solar plasma raypath separations at 1 AU scale height

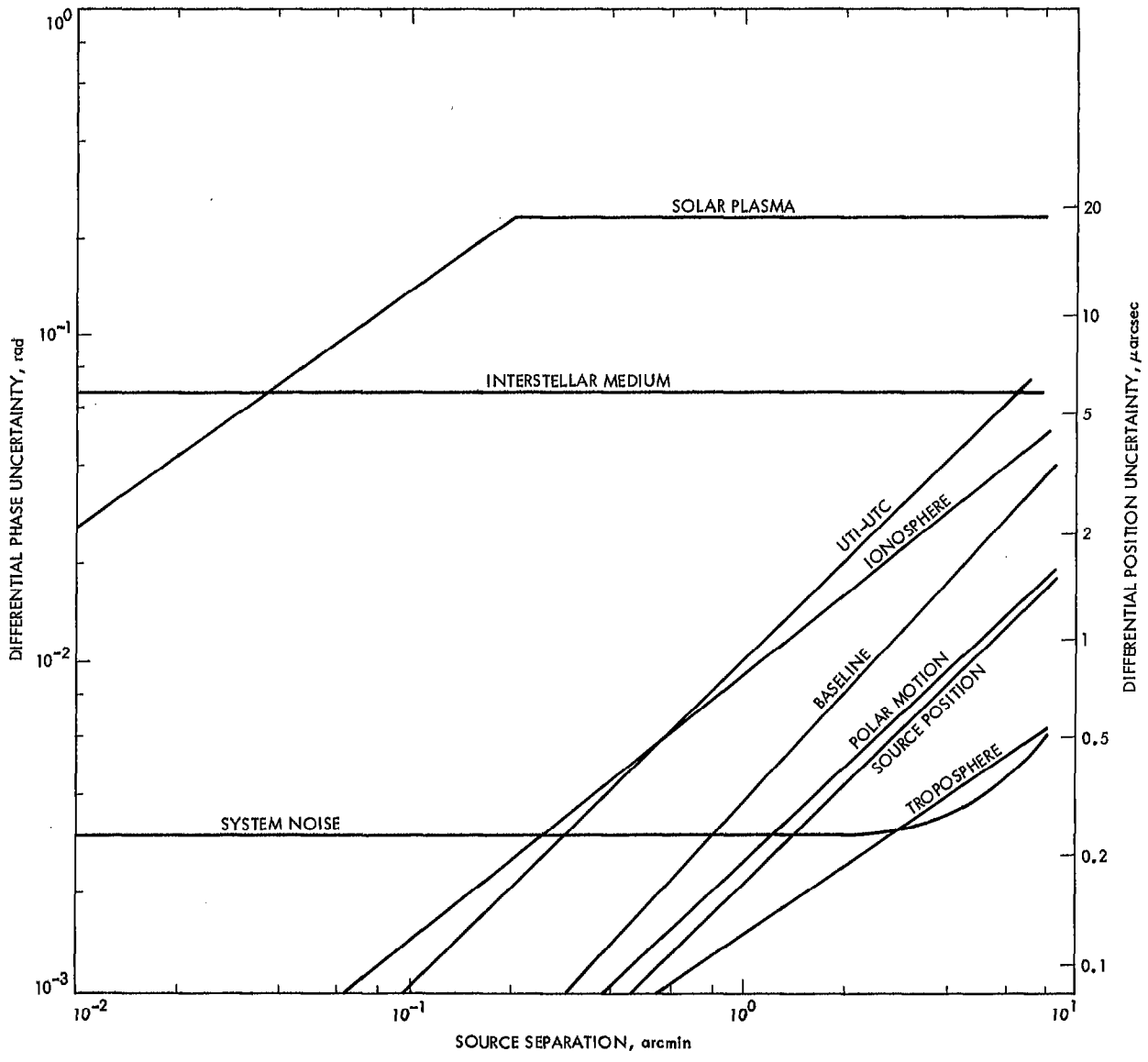

Fig. 4. S-band SVLBI errors vs angular separation between sources

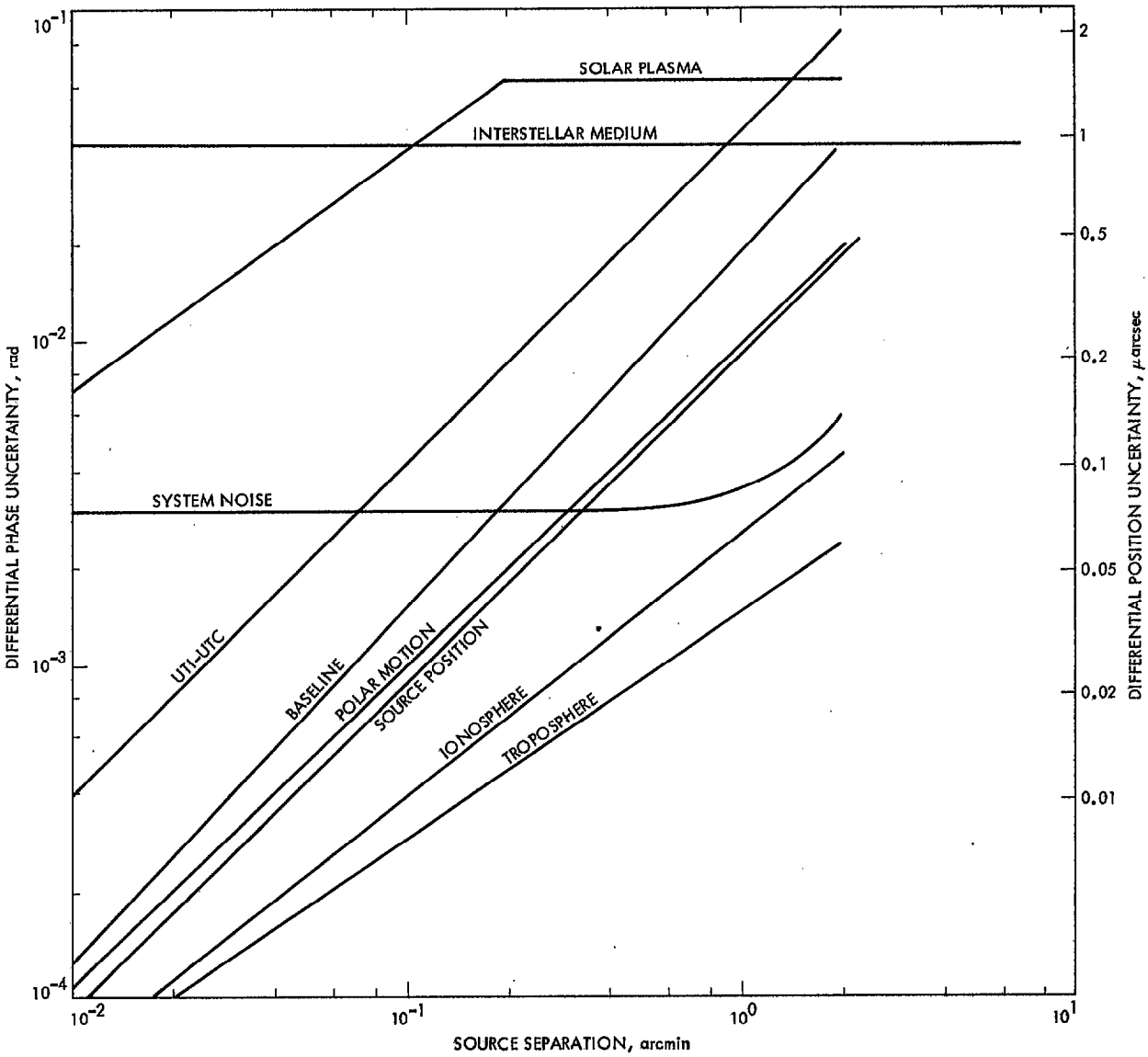

Fig. 5. X-band SVLBI errors vs angular separation between sources

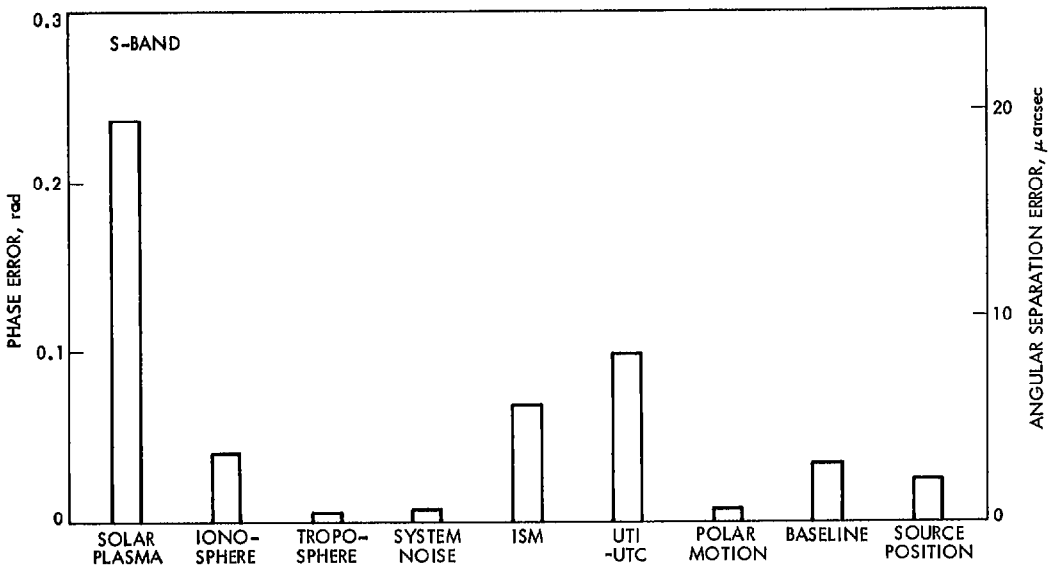

Fig. 6. S-band error bar chart for GC 1342+66

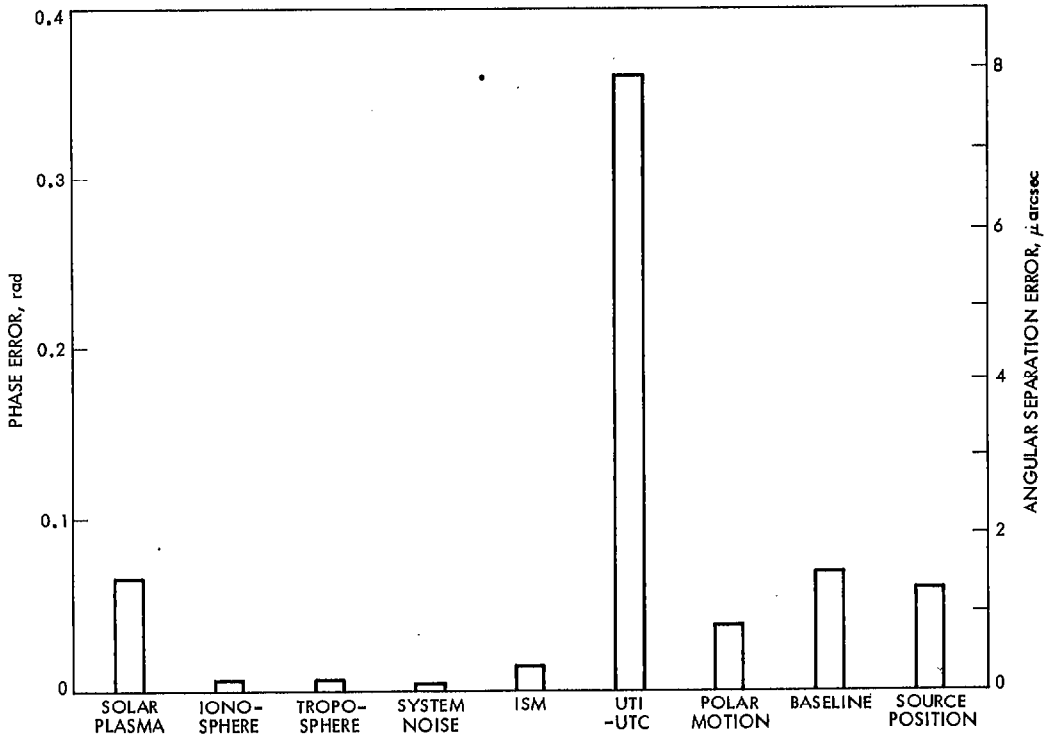

Fig. 7. X-band error bar chart for GC 1342+66